Sensitized near infrared emission of g-C_3N_4: Yb^{3+} composite

WENBIN XIA, GUOJUN ZHU, XUE JUN GAO, XIANGLIANG JIN, XIAOLIANG YANG*, SIGUO XIAO
School of Physics and Optoelectronics, Xiangtan University, Hunan 411105, China

g-C_3N_4: Yb^{3+} composite has been prepared by a simple method using melamine and $YbCl_3$ as raw materials. The introduced Yb^{3+} ions are composited with g-C_3N_4 and significantly cause the crystal lattice distortion in g-C_3N_4, which is supported by first principles calculation and XRD patterns. The g-C_3N_4: Yb^{3+} composite can absorb blue-violet light and give near-infrared light at around 1 μm. Energy transfer sensitization from g-C_3N_4 to Yb^{3+} is demonstrated on the base of the excitation and emission spectra. The result refers a new approach for conversion of short wavelength light into near infrared emission.

(Received September 12, 2016; accepted August 9, 2017)

Keywords: Rare-earth, Graphitic-C_3N_4, Sensitization, Structure distortion, First principle method

1. Introduction

Trivalent rare earth ions (RE^{3+}) doped luminescence and laser materials in various forms such as glass, crystal and nano powder are of interest not only for basic research, but also for practical application [1-6]. Among the rare earth ions, the Yb^{3+} ion has the simplest energy level scheme, constituting of only two $^2F_{5/2}$ and $^2F_{7/2}$ levels [7]. There is no excited state absorption, no cross-relaxation process and no more up-conversion internal mechanism able to reduce the effective emission cross section. Therefore, Yb^{3+} ion is commonly considered as an activator ion of big prospect for construction of laser and luminescence materials operating at about 1μm. Regretfully, the f-f transitions of Yb^{3+} ion is Laporte forbidden with low absorption coefficients, which limits its pump efficiency. Sensitization might be an effective pathway to increase the 4f-4f absorption of Yb^{3+} and then makes luminescence generation more efficient. The photoluminescence properties of Yb^{3+} ions sensitized by other rear earth ions like Er, Tb, Pr, Tm, Ho and Ce [6, 8-16] have been widely reported. However, the narrow absorption bands and weak absorption efficiencies of these sensitizing ions result in the unsatisfactory sensitization effect.

As we know, the semiconductors with direct band gap have strong absorption in short wavelength region. It is believed that the direct band gap semiconductors could act as both host and ideal sensitizer of Yb^{3+}, enhancing the excitation efficiency of the Yb^{3+} doped semiconductor phosphors. These near infrared emitting Yb^{3+} doped semiconductor phosphors are attractive because they have wide potential applications in many fields such as lasers [17, 18], solar spectral converters [19, 20], and biological fluorescent probes, [21, 22] etc. In previous studies, the Yb^{3+} near-infrared emission sensitized by semiconductor such as InP, GaP and GaAs were observed. But in those semiconductor, the low doping contention leads to the relatively weak luminescence intensity of Yb^{3+} emission [23, 24].

In the recent years, graphitic carbon nitride (g-C_3N_4) as one of carbon semiconductors has also been widely studied because of its unique combination of various physicochemical properties such as semi-conductivity, special optical feature, energy-storage capacity, and gas-adsorption capacity. [25-29] It is noted that the direct band gap semiconductor graphene-like g-C_3N_4 has good thermal and chemical stability and has large specific surface area and porosities[30] with large number of active chemical sites on the surface and uniform pore size. Especially, the moderate bandgap energy (2.95 eV) means that it can efficiently absorb the blue-violet light. At the meantime, relatively high content of Yb^{3+} ions are probably inserted into the interstitial positions of g-C_3N_4 by coordinating to the N atoms when the Yb^{3+} ions are introduced into the g-C_3N_4 matrix. [29, 31, 32] Thus the luminous energy absorbed by g-C_3N_4 might be transferred to enough Yb^{3+} ions in the Yb^{3+} doped g-C_3N_4 material, resulting in strong luminescence at about 1μm. So it is predicted that g-C_3N_4: Yb^{3+} composite might be a good near infrared phosphor.

In this paper, the g-C_3N_4 was prepared by calcining melamine. Then the g-C_3N_4: Yb^{3+} composite was prepared by liquid-phase synthesis method. In order to reveal the position of the doped Yb^{3+} ions in g-C_3N_4 and their influence on g-C_3N_4 structure, first-principles simulations and XRD measurement have been performed. Near infrared emission originating from Yb^{3+} sensitized by C_3N_4 is demonstrated in the g-C_3N_4: Yb^{3+} composite.

2. Experimental

2.1. Materials synthesis

Sample preparation included the following steps. Firstly, the g-C_3N_4 bulk material was obtained by calcining melamine at 550 °C for 4h and the prepared g-C_3N_4 bulk material was ground for 1h in a ball mill with zirconia

balls. Then a certain amount of g-C_3N_4 power obtained was put into water and ultrasonically treated for 2 h. After being stirred with a magnetic stirrer for 12 h, bulk g-C_3N_4 was exfoliated into thin sheets and disintegrated into a homogeneous suspension. Then the $YbCl_3$ solution was instilled into the suspension and stirred at room temperature for 30 min. The g-C_3N_4 and $YbCl_3$ mixed suspension was dried at 100 °C in air to obtain the precursor. Finally the precursor was calcined at 400 °C for 1h and the target g-C_3N_4: Yb^{3+} composite was obtained when it cooled down to room temperature.

2.2. Characterization

The crystal structure of samples were measured by X-ray diffraction (XRD) on a Bruker D8 advanced equipment using Cu tube with Cu/K (k = 0.1541 nm) radiation. The morphology of the synthesized samples was characterized using a JEM-2100 transmission electron microscopy (TEM) operating at accelerating voltage of 200 kV. X-ray photoelectron spectroscopy (XPS) was measured on a K-Alpha 1063 (Thermo Fisher Scientific) with a focused monochromatic Al Ka X-ray beam (12 kV, 6 mA, 5×10^{-9} torr). The excitation and visible-near-infrared emission spectra were measured with an FLS920 (Edinburgh) Spectrometer at room temperature. In order to guarantee the accuracy of experimental data, the spectroscopic measurement condition was kept consistent for all the samples.

3. Results and discussion

The X-ray diffraction (XRD) patterns of g-C_3N_4: Yb^{3+} samples with different Yb^{3+} content are shown in Fig. 1. The diffraction pattern of each sample shows the strongest diffraction peak at 27.40° corresponding to the (002) interplanar (lattice distance = 0.326 nm), which is well-known for graphite-like packing characteristic of g-C_3N_4 materials.[33, 34] The weak peak at 13.12° can be assigned to (100) in-planar that arises from the in-plane ordering of tri-s-triazine units.[33, 34] It can be seen from the Fig. 1 that the diffraction (XRD) patterns of prepared g-C_3N_4: Yb^{3+} samples mainly shows the peaks of pure g-C_3N_4 and no impurity of other Ytterbium compound is observed. Moreover, no shift of diffraction peak position has been observed with the introduction of Yb^{3+}, even at relative high Yb^{3+} concentration that the molar ratio of Yb^{3+}: C_3N_4 reaches to 0.4. This indicates that the introduced Yb^{3+} ions have been composited with g-C_3N_4 and have not changed the basic structure of C_3N_4. However, it is found that the peak at 27.40° tends to weaken when the Yb^{3+} content increases. Additionally, the full width at half maximum (FWHM) is also broadens with Yb^{3+} content increasing. The value of FWHM of the pure g-C_3N_4 is about 2.29 degree, and the value of FWHM increases from 2.54 to 2.83 degree with Yb^{3+} content increasing from 0.1 to 0.4. Those results suggest that the introduced Yb^{3+} ions can significantly cause the crystal lattice distortion in g-C_3N_4.

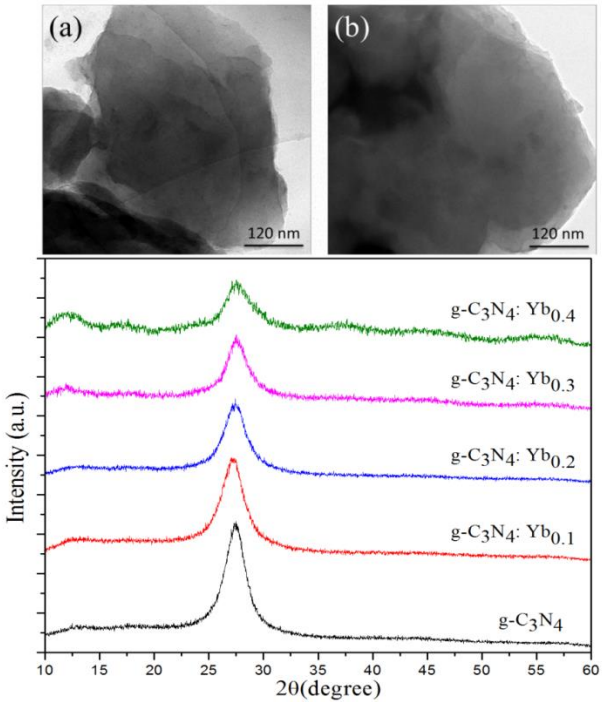

Fig. 1. TEM images of g-C_3N_4: $Yb_{0.2}$ sample. Power X-ray diffraction patterns of g-C_3N_4: Yb_x (x=0.0, 0.1, 0.2, 0.3, 0.4) samples

The TEM images of the g-C_3N_4: Yb^{3+} composite are shown in Fig. 1. The TEM images show that the prepared composite have a smooth planar structure. This structure has a large specific surface and porosities, which is benefit for the adsorption of RE^{3+} ions in g-C_3N_4. The XPS of g-C_3N_4: $Yb_{0.2}$ was measured to examine the valence state of Yb element in the composite. According to the smoothed XPS curve shown in Fig. 2, the core level binding energy of Yb_{4d} is estimated to be about 186 eV, similarly to the binding energy of Yb_{4d} in Yb_2O_3. [35] This means that the Yb element predominantly behaves as the state of Yb^{3+} in the g-C_3N_4: Yb^{3+} composite.

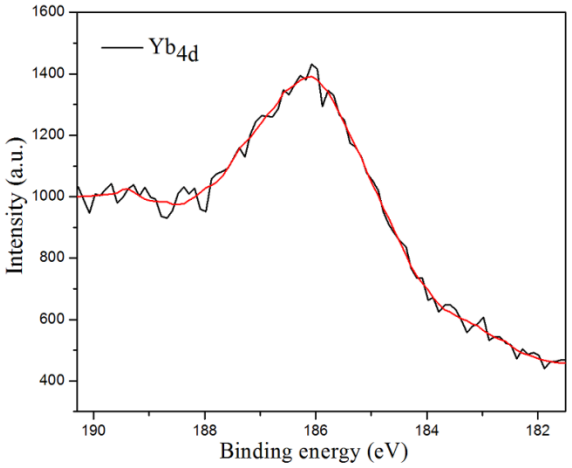

Fig. 2. Yb_{4d} XPS spectrum of g-C_3N_4: $Yb_{0.2}$ sample

In fact, the ionic radius of Yb^{3+} is much larger than that of C and N. Therefore, it is difficult for the Yb^{3+} ions to enter the g-C_3N_4 lattice by substitutional doping. The previous studies of Fe/Ce/Co-doped g-C_3N_4 suggest that Fe, Ce and Co are inserted into the interstitial position of g-C_3N_4 and stabilized in the electron-rich g-C_3N_4 structure mainly through Fe/Ce/Co-N bonds [32, 36, 37].

To better understand the possible position of Yb^{3+} in the g-C_3N_4: Yb^{3+} composite, a first-principles study on the structure properties of Yb atoms absorbed g-C_3N_4 monolayer has also been performed. To simulate the interaction between the adatoms and the g-C_3N_4 sheet, the structure of Yb atom absorbed g-C_3N_4 was mimicked as a super cell composed of 2×2 g-C_3N_4 super-cell with one Yb atom placed on 3Å over the g-C3N4 plane (Fig. 3 (a) (b)). The molar ratio of Yb^{3+}: C_3N_4 was taken as 0.25 for simplify the calculation.

The first-principle calculations were carried out with the Vienna ab-initio simulation package (VASP)[16, 38], based on spin-polarized density functional theory (DFT). The interaction between valence electrons and ionic cores was described within the framework of the projector augmented wave (PAW) method [9, 39]. The spin-polarized generalized gradient approximation (GGA) was used for the exchange-correlation potential in the form proposed by Perdew, Burke, and Ernzerhof (PBE) [15]. To mimic the appropriate environment for an isolated sheet, we used a slab model that has periodic boundary conditions with a vacum space of 20 Å along the z axis direction. The structures were fully relaxed using the conjugated gradient method. For the Brillouin zone sample, the reciprocal space was prensented by the Monkhost-Pack special k-points method [40] of 3×3×1 mesh for geometry relax, and 6×6×1 mesh for static calculation. And the convergence criteria were set to 1×10^{-5}eV and 0.05eV/Å for energy and Hellman-Feynman forces, respectively. The energy cutoff for the plane wave basis expansion was set to 450eV. The lattice constant of the unit cell for the g-C_3N_4 monolayer was select to 7.135 Å, which was consistent with previous studies [41, 42]. As shown in Fig. 3(a), there we selected three representative sites for Yb to simulate the interaction between the adatoms and the g-C_3N_4 sheet, and the Yb atoms were initially placed on 3Å over the g-C_3N_4 plane in this three different situations. After full relaxation, the Yb moved to a relatively stable position. Only in the case that Yb was placed in C site, the Yb fell into the pore site, inserted in interstitial position of g-C_3N_4 sheet, as shown in the schematic diagram in Fig. 3(c). While in the remaining cases the Yb was still around 2Å over the g-C_3N_4 plane after full relaxation.

The stabilities of the Yb atoms on g-C_3N_4 can be estimated through their total energy of whole system consisting of Yb and g-C_3N_4. The total energies is -117.87438eV, -118.21376eV and -122.64826eV in the case of A, B and C, respectively. Obviously, site with the minimum total energy is referred to as the favored site. Therefore, the pore site (C1) is the most possible position of the three adsorption sites considered. The result suggests that the Yb^{3+} ions are most likely inserted into the interstitial position of g-C_3N_4. It is also noticed that original coplanar C and N atoms deviate from the plane along the z axis direction when an Yb^{3+} ion is inserted the interstitial position (C1 site) of g-C_3N_4 according to the simulation results. The maximum deviation is about 1.03Å. This means that the doped Yb^{3+} ions have caused severe structural distortion of g-C_3N_4 monolayer, just as show in Fig. 3(c) (d). The simulation results are identical with the XRD measurement.

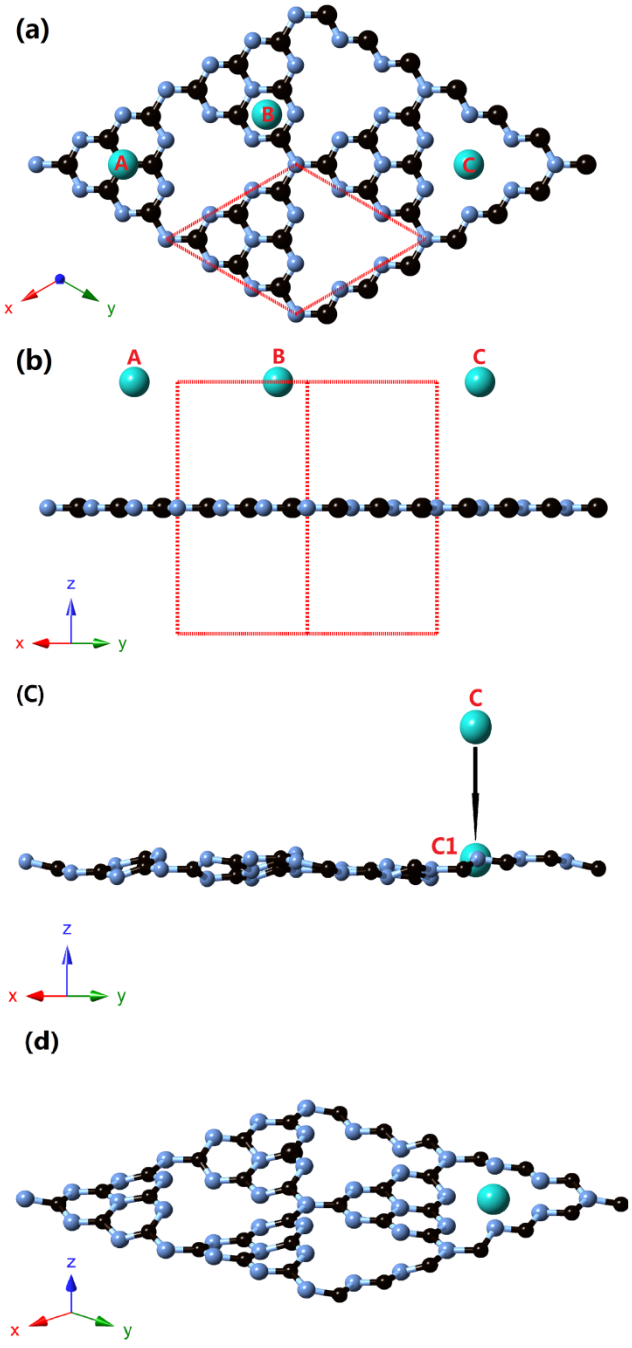

Fig. 3. The structure diagrams of Yb doped g-C_3N_4 sheet, top view (a) and side view (b) of the initial structure; side view (c) of relaxation processes diagram; (d) is bird's eye view, the structure of Yb at C1 site after relaxation. Here the black, blue, and blue-green spheres represent carbon, nitrogen, and ytterbium atoms, respectively

The diffuse reflection spectra of g-C_3N_4: Yb_x (x=0.0, 0.1, 0.2, 0.3) is presented in Fig. 4(a). It can be seen that the composite has a strong absorption of the blue-violet light. There also exists "red shift" phenomenon for the diffuse reflection spectra of g-C_3N_4 with the doping of Yb^{3+} ion, which might be caused by lattice distortion of g-C_3N_4 or the generation of defects in the band gap of g-C_3N_4 during the process of compositing the g-C_3N_4 and Yb^{3+}.

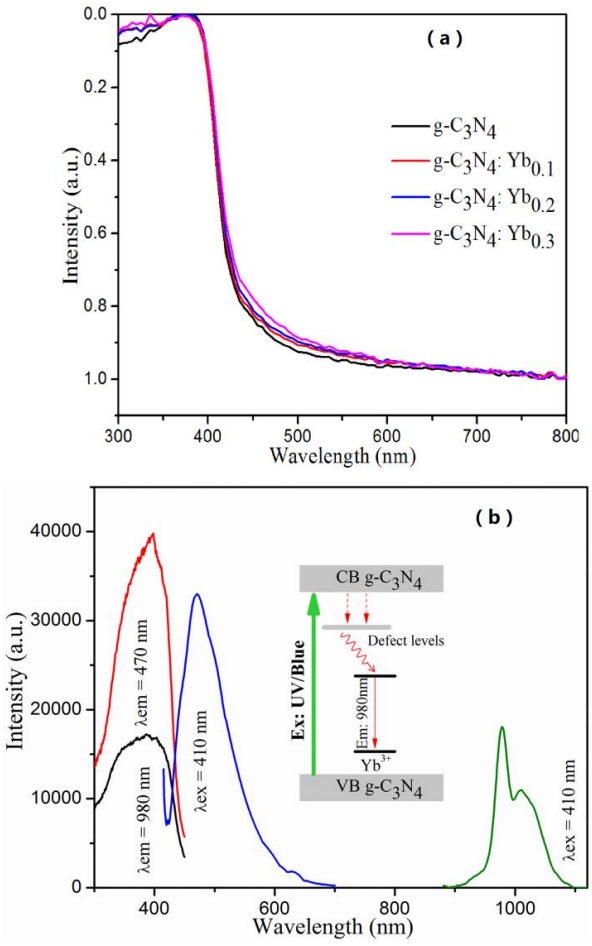

Fig. 4. (a) Diffuse reflection spectra of g-C_3N_4: Yb_x (x=0.0, 0.1, 0.2, 0.3) samples. (b). The excitation and emission spectra of the g-C_3N_4: $Yb_{0.2}$ sample, and the energy-transfer and electron-transition scheme of g-C_3N_4 and Yb^{3+}

As shown in Fig. 4(b), excited into its absorption band by wavelength of 410 nm, pure g-C_3N_4 gives an intense broad emission band in range of 420 nm-650 nm. The excitation spectrum monitored at 470 nm of pure g-C_3N_4 sample shows a broad excitation spectra band ranging from ultraviolet to 420 nm, corresponding well with its absorption region. In the g-C_3N_4: $Yb_{0.2}$ composite, the excitation at 410 nm can give a new luminescence band locating at 980 nm emitted by Yb^{3+}. It is noteworthy that the shape of the excitation spectrum of the g-C_3N_4: $Yb_{0.2}$ composite monitored at 980 nm is quite similar to that of pure g-C_3N_4 sample monitored at 470 nm (see Fig. 4(b)). The result indicates that the energy transfer from g-C_3N_4 to Yb^{3+} occurs when g-C_3N_4 has been excited. The results suggest that the g-C3N4: Yb^{3+} can convert light in blue-violet region into the near-infrared emission.

Based on the diffuse reflection spectra (Fig. 4(a)), the band gap of g-C_3N_4 is estimated to 2.95 eV. Therefore, the luminescence of g-C_3N_4 might be ascribed to the radiative transition originating from defect levels in the band gap of g-C_3N_4. Firstly, the electrons are excited into conduction band by the irradiation of the blue-violet light, and then the excited electrons rapidly relax to the defect levels in the band gap. Then blue emission occurs by electron transition from defect levels to valence band. When the Yb^{3+} ions are inserted into the interstitial position of g-C_3N_4, the energy absorbed by g-C_3N_4 can be transferred to Yb^{3+}. The Yb^{3+} ions are excited to their $^2F_{5/2}$ states in the energy transfer between the defect levels of g-C_3N_4 and Yb^{3+} ions. When the Yb^{3+} ions at excited states return to their ground states, near-infrared light at around 980 nm emits. The mechanism of near-infrared emission of Yb^{3+} sensitized by g-C_3N_4 in the g-C_3N_4: $Yb_{0.2}$ composite is illustrated in Fig. 4(b).

4. Conclusions

In this work, g-C_3N_4: Yb^{3+} composite has been prepared. The g-C_3N_4: Yb^{3+} composite exhibits strong absorption of blue-violet light and the energy transfer sensitization of g-C_3N_4 to Yb^{3+} can give near-infrared emission of Yb^{3+} at around 1μm. The investigation provides a meaningful new material that can convert light from short wavelength region to near-infrared one, which opens up possibilities for application such as solar spectral conversion and blue-violet light detection.

Acknowledgements

This work was supported by the National Natural Science Foundation of China (No. 51372214 & 61233010).

References

[1] X. Wang, J. Zheng, Y. Xuan, X. Yan, Opt. Express **21**(18), 21596 (2013).
[2] X. Wang, Q. Liu, Y. Bu, C.-S. Liu, T. Liu, X. Yan, RSC Advances **5**(105), 86219 (2015).
[3] X. Chen, J. Zhao, L. Yu, C. Rong, C. Li, S. Lian, Journal of Luminescence **131**, 2697 (2011).
[4] V. B. Taxak, R. Kumar, J. K. Makrandi, S. P. Khatkar, Displays **30**, 170 (2009).
[5] V. B. Taxak, S. P. Khatkar, S. D. Han, R. Kumar, M. Kumar, Journal of Alloys & Compounds **469**, 224 (2009).
[6] H. J. Seo, W. Jing, Q. Lin, P. Cai, T. Vu, X. Wang, X. Yan, Y. Bu, Optics Letters **41**(22), 5314 (2016).
[7] X. Wang, S. Xiao, X. Yang, J. Ding, Journal of

Materials Science **43**(4), 1354 (2008).
[8] X. Wang, Q. Liu, P. Cai, J. Wang, L. Qin, T. Vu, H. J. Seo, Opt. Express **24**(16), 17792 (2016).
[9] D. E. Van, M. Bryan, L. Aarts, A. Meijerink, Advanced Materials **21**(30), 3073 (2009).
[10] X. Liu, S. Ye, Y. Qiao, G. Dong, B. Zhu, D. Chen, G. Lakshminarayana, J. Qiu, Applied Physics B **96**(1), 51 (2009).
[11] K. Deng, T. Gong, L. Hu, X. Wei, Y. Chen, M. Yin, Optics Express **19**(3), 1749 (2011).
[12] D. C. Yu, X. Y. Huang, S. Ye, Q. Y. Zhang, Journal of Alloys & Compounds **509**, 9919 (2011).
[13] J. D. Chen, H. Guo, Z. Q. Li, H. Zhang, Y. X. Zhuang, J. D. Chen, H. Guo, Z. Q. Li, H. Zhang, Y. X. Zhuang, Optical Materials **32**, 998 (2010).
[14] L. Lin, H. Lin, Z. Wang, J. Chen, R. Huang, X. Rao, Z. Feng, Z. Zheng, Optical Materials **36**, 1065 (2014).
[15] X. Wang, C. S. Liu, T. Yu, X. Yan, Physical Chemistry Chemical Physics **16**(26), 13440 (2014).
[16] X. Huang, D. Chen, L. Lin, Z. Wang, Optik - International Journal for Light and Electron Optics **125**, 565 (2014).
[17] Y. Ren, G. Brown, A. Ródenas, S. Beecher, F. Chen, A. K. Kar, Optics Letters **37**(16), 3339 (2012).
[18] A. A. Lagatsky, O. L. Antipov, W. Sibbett, Opt. Express **20**(17), 19349 (2012).
[19] B. Fan, C. Chlique, O. Merdrignac-Conanec, X. Zhang, X. Fan, The Journal of Physical Chemistry C **116**(21), 11652 (2012).
[20] T. C. Liu, G. Zhang, X. Qiao, J. Wang, H. J. Seo, D. P. Tsai, R. S. Liu, Inorg. Chem. **52**(13), 7352 (2013).
[21] N.-N. Dong, M. Pedroni, F. Piccinelli, G. Conti, A. Sbarbati, J. E. Ramírez-Hernández, L. M. Maestro, M. C. Iglesias-de la Cruz, F. Sanz-Rodriguez, A. Juarranz, ACS Nano **5**, 8665 (2011).
[22] G. Chen, J. Shen, T. Y. Ohulchanskyy, N. J. Patel, A. Kutikov, Z. Li, J. Song, R. K. Pandey, H. Ågren, P. N. Prasad, ACS Nano **6**(9), 8280 (2012).
[23] W. Körber, A. Hangleiter, Applied Physics Letters **52**(2), 114 (1988).
[24] H. Ennen, G. Pomrenke, A. Axmann, Journal of Applied Physics **57**(6), 2182 (1985).
[25] X. L. Zhang, C. Zheng, S. S. Guo, J. Li, H. H. Yang, G. Chen, Anal. Chem. **86**(7), 3426 (2014).
[26] L. Xu, W.-Q. Huang, L.-L. Wang, Z.-A. Tian, W. Hu, Y. Ma, X. Wang, A. Pan, G.-F. Huang, Chemistry of Materials **27**(5), 1612 (2015).
[27] X. Zhang, X. Xie, H. Wang, J. Zhang, B. Pan, Y. Xie, J. Am. Chem. Soc. **135**(1), 18 (2013).
[28] Q. Xiang, J. Yu, M. Jaroniec, The Journal of Physical Chemistry C **115**(15), 7355 (2011).
[29] S. Min, G. Lu, The Journal of Physical Chemistry C **116**(37), 19644 (2012).
[30] S. S. Park, S. W. Chu, C. Xue, D. Zhao, C. S. Ha, Journal of Materials Chemistry **21**(29), 10801 (2011).
[31] X. Chen, J. Zhang, X. Fu, M. Antonietti, X. Wang, Journal of the American Chemical Society **131**(33), 11658 (2009).
[32] R. Jin, S. Hu, J. Gui, D. Liu, Bulletin of the Korean Chemical Society **36**(1), 17 (2015).
[33] D. Jiang, J. Zhu, M. Chen, J. Xie, Journal of Colloid and Interface Science **417**, 115 (2014).
[34] D. Jiang, L. Chen, J. Zhu, M. Chen, W. Shi, J. Xie, Dalton Transactions **42**(44), 15726 (2013).
[35] T.-M. Pan, C.-H. Cheng, C.-D. Lee, Journal of The Electrochemical Society **156**(5), J108 (2009).
[36] Q. Liu, J. Zhang, Langmuir **29**(11), 3821 (2013).
[37] X. Wang, X. Chen, A. Thomas, X. Fu, M. Antonietti, Metal-Containing Carbon Nitride Compounds: A New Functional Organic–Metal Hybrid Material, Advanced Materials **21**(16), 1609 (2009).
[38] X. Wang, J. Zheng, Y. Xuan, X. Yan, Opt. Express **21**(18), 21596 (2013).
[39] P. E. Blöchl, Physical Review B **50**(24), 17953 (1994).
[40] H. J. Monkhorst, J. D. Pack, Physical Review B **13**(12), 5188 (1976).
[41] Y. Zhang, Z. Wang, J. Cao, Journal of Materials Chemistry C **2**(41), 8817 (2014).
[42] Q. Liu, J. Zhang, Langmuir **29**(11), 3821 (2013).

*Corresponding author: xiaoliangy@xtu.edu.cn